

# Role of the substrate in electronic structure, molecular orientation, and morphology of organic thin films: diindenoperylene on rutile TiO<sub>2</sub>(110)

Britt-Elfriede Schuster,<sup>a</sup> M. Benedetta Casu,<sup>\*a</sup> Indro Biswas,<sup>a</sup> Alexander Hinderhofer,<sup>b</sup> Alexander Gerlach,<sup>b</sup> Frank Schreiber<sup>b</sup> and Thomas Chassé<sup>a</sup>

Received 29th June 2009, Accepted 5th August 2009

First published as an Advance Article on the web 18th August 2009

DOI: 10.1039/b912790a

**The results of our multitechnique investigation performed on diindenoperylene thin films deposited on rutile TiO<sub>2</sub>(110) show island growth, with crystallites nucleating preferentially along the [1 $\bar{1}$ 0] substrate crystallographic axis. The findings evidence that the films' properties at the interface are common to those found for a number of organic molecules deposited on the same substrate, revealing that the structural and morphological properties of organic thin films on rutile TiO<sub>2</sub>(110) are completely driven by its surface morphology.**

In the past organic materials were considered very appealing not only because of a pure academic interest but also because of their promising characteristics towards electronic applications.<sup>1</sup> Nowadays we can affirm that these materials kept their promises and they are widely present on the market. Some of their properties demand deeper investigation and a better understanding, also in view of their use in an even larger number of applications, where low costs, chemical flexibility and energy saving technologies play a major role and organic molecules may achieve a different or a better performance than inorganic semiconductors.<sup>2</sup> Organic thin films properties like morphology, structure, and electronic structure are strongly influenced by preparation conditions, the substrate, and post-growth treatment.<sup>3–5</sup> Among small molecules, the most investigated ones, because of their importance as a model system and as an active layer in devices, are certainly the acenes, the phthalocyanines, and the perylene-based molecules.<sup>6,7</sup> Diindenoperylene (DIP, C<sub>32</sub>H<sub>16</sub>, Fig. 1) is a perylene-based molecule that shows a high hole mobility already in thin films,<sup>8</sup> good film forming properties and thermal stability.<sup>9–13</sup> Thus, DIP is a molecule that can be used as a model system but at the same time it is very promising from a technological point of view. Titanium dioxide is an optically clear insulating oxide, and it is the most investigated single crystalline system among all metal oxides.<sup>14</sup> The rutile TiO<sub>2</sub>(110) surface is the most stable surface configuration. The application potential is enormous, ranging from medicine to electronics.<sup>14,15</sup> Besides the interest in the investigation of a new organic/oxide system, it is clear how the coupling of two such excellent materials may also lead to further steps in device engineering.

Here, we report the results of a multitechnique investigation performed on DIP thin films deposited on rutile TiO<sub>2</sub>(110). We have found evidence for island growth, with DIP crystallites nucleating preferentially along the [1 $\bar{1}$ 0] crystallographic axis of the substrate. In thicker films, the molecules assume an upright standing configuration.

Sample preparation and photoemission experiments (X-ray photoelectron spectroscopy, XPS) were carried out in an ultrahigh vacuum (UHV) system consisting of two preparation chambers (base pressure better than 10<sup>−9</sup> mbar), and an analyzing chamber (base pressure of around 5 × 10<sup>−10</sup> mbar) equipped with a low energy electron diffraction (LEED) system, a SPECS Phoibos 100 analyzer, and a monochromatized X-ray source (Focus 500, XR50M X-ray source, Al K $\alpha$  1486.74 eV). A clean carbon-free rutile TiO<sub>2</sub>(110) single crystal (PI-KEM Ltd, United Kingdom) was prepared by a very gentle and brief Ar<sup>+</sup> ion bombardment (500 V), followed by annealing in UHV at approximately 830 K, which gave a sharp LEED pattern of an (1 × 1) reconstruction.<sup>16</sup> After several cycles of sputtering and annealing the crystal showed a pale blue color, a convenient indicator for the concentration of bulk oxygen vacancies and the associated color centers. The Ti 2p core level photoemission spectrum showed only a very weak low binding energy shoulder usually attributed to the presence of surface non-stoichiometry due to oxygen vacancies (3–5% in our clean substrates). The root mean square (rms) roughness of the bare substrate after preparation was 11 nm. Thin films of DIP were prepared *in situ* by organic molecular beam deposition (OMBD) using strictly controlled evaporation conditions (evaporation rate = 3 Å min<sup>−1</sup>, T<sub>sub</sub> = 20 °C). The nominal thicknesses were measured with a quartz crystal microbalance and were cross-checked by using the attenuation of the XPS substrate signal after DIP deposition. Survey XPS spectra were recorded using a pass energy of 30 eV, detailed spectra were performed with a pass energy of 10 eV resulting in an experimental resolution of 450 meV. All spectra were calibrated to the Ti 2p<sub>3/2</sub> emission of the substrate. Atomic force microscopy (AFM) measurements were performed under ambient conditions in tapping mode with a Nanoscope IIIa (Digital Instruments) scanning probe microscope. Near edge X-ray absorption spectroscopy (NEXAFS) measurements were performed at the beamline UE52-PGM at BESSY (Berlin). This beamline is characterized by a plane grating monochromator. The photon energy ranges from 100 to 1500 eV, with an energy resolving power of E/ $\Delta$ E = 10 500 at 401 eV (c<sub>ff</sub> = 10, 10  $\mu$ m exit slit). The main chamber (base pressure 2 × 10<sup>−10</sup> mbar) is equipped with a standard twin

<sup>a</sup> Institute of Physical and Theoretical Chemistry, University of Tübingen, Auf der Morgenstelle 8, 72076 Tübingen, Germany. E-mail: benedetta.casu@uni-tuebingen.de;

Fax: +49 (0)7071 29 5490; Tel: +49 (0)7071 29 76252

<sup>b</sup> Institute for Applied Physics, University of Tübingen, Auf der Morgenstelle 10, 72076 Tübingen, Germany

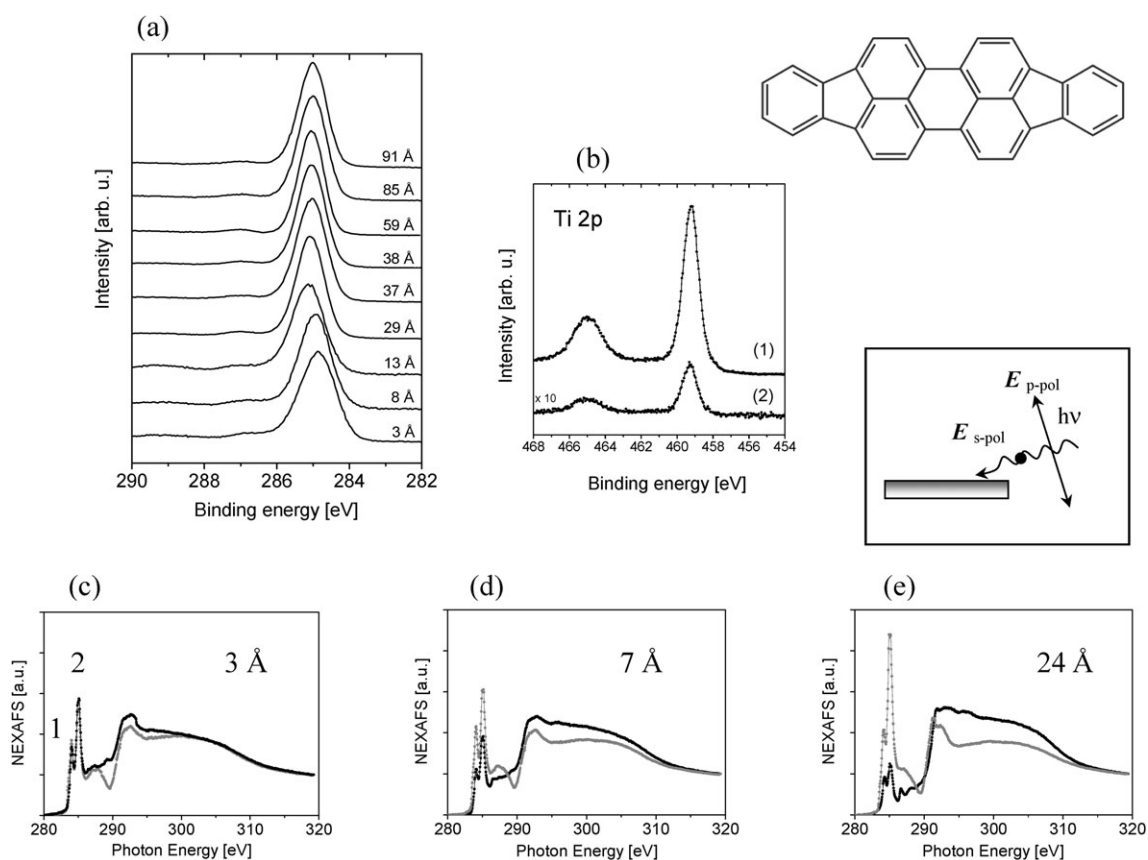


**Fig. 1** (a) Thickness-dependent C 1s core level photoemission spectra of DIP deposited on rutile (110) are shown. (b): Ti 2p core level photoemission spectra of rutile  $\text{TiO}_2(110)$  as prepared (1) and after deposition of a DIP film (nominal thickness: 91 Å) (2). C 1s NEXAFS spectra obtained from 3 (c), 7 (d) and 24 Å (e) of DIP thin films deposited on  $\text{TiO}_2(110)$  at RT. The spectra were taken in grazing incidence for p- (black curve) and s- (grey curve) polarisation. The geometry of the NEXAFS experiment and the molecular structure are also shown.

anode X-ray source, a SCIENTA R4000 electron energy analyzer, and a home-made partial electron yield detector.

The X-ray reflectivity measurements were made *ex situ* with a two-circle instrument (XRD, 3003 TT, Seifert Analytical X-ray). Using a X-ray tube with a copper anode and a Ni/C multilayer mirror in combination with a germanium channel-cut crystal gives a monochromatic and parallel beam with  $\lambda = 1.54 \text{ \AA}$  (Cu  $\text{K}_{\alpha 1}$ ). The chosen slits in front of the scintillation counter resulted in an angular resolution of  $\sim 0.01^\circ$ , and a dynamic range of more than seven orders of magnitude. All films were carefully checked for radiation damage during data acquisition. No degradation of the samples was observed on the time scale of all performed experiments.

XPS is a very powerful technique to gain information about electronic structure and chemical bonding. In Fig. 1a the thickness-dependent C 1s core level photoemission spectra of DIP deposited on  $\text{TiO}_2(110)$  are shown. A strong peak dominates the spectrum at 285.0 eV in the thicker films, and a smaller shake-up satellite at 287.0 eV is clearly visible. The peaks stem from the C 1s core levels. Considering the DIP molecular structure, at first two contributions from different carbon sites can be expected, namely, the carbon atom sites that belong to the aromatic rings surrounded by adjacent carbon atoms, and the remaining carbon sites (C–H bonds). In principle, because of the molecular symmetry (the free

diindenoperylene molecule belongs to the  $D_{2h}$  point group), the C 1s core level features are expected to be due to at least nine contributions, one for each different non-equivalent carbon site. However, due to their similar binding energy and the finite resolution of our experiment their separation and energy determination by curve fitting would be quite speculative. The shake-up satellite at 287.0 eV (HOMO–LUMO shake up satellite) is already clearly visible for the first layer deposited on top of the  $\text{TiO}_2$  surface. Its relative intensity does not change relevantly with thickness indicating that the satellite is due to intramolecular screening effects of the core hole.<sup>17</sup> Comparing its separation from the main C 1s peak, we observe that it is lower than the DIP optical gap.<sup>13</sup> This suggests that the HOMO–LUMO shake up excitations contribute to screen the core hole *via* a charge distribution within the molecule, as seen in polyacenes, due to the delocalization of the charge in the aromatic system.<sup>18</sup> In addition, a 0.2 eV energy shift of the C 1s peak towards higher binding energies with increasing film thickness is observable. This relatively small shift confirms a poor screening effect of the C 1s core hole depending on the substrate and is in agreement with the insulating nature of the substrate.<sup>17</sup> Another observed effect is the decrease of the line width with increasing film thickness. There are several contributions that affect the line shapes in XPS spectra of large  $\pi$ -conjugated organic molecules, like intrinsic lifetime broadening, experimental

contributions, and vibronic and inhomogeneous broadening.<sup>19</sup> In this case, most of these contributions (*e.g.* lifetime, experimental set up) are constant for each presented curve, thus the difference in line width indicates a different strength of the interaction among the molecules in the few layers up to 20 Å (*e.g.* different molecular packing and/or orientation). In particular, the larger full width at half maximum (FWHM) of the C 1s peak for thinner films (FWHM = 1.1 eV) indicates a stronger inhomogeneity of the first layers on top of the substrate with respect to the successive layers (FWHM = 0.9 eV). Thickness dependent XPS investigations offer also the opportunity to identify the growth mode.<sup>20</sup> Thus, we have simultaneously monitored the C 1s and the Ti 2p core levels with XPS during growth. In Fig. 1b, the Ti 2p core level signals are shown, upon deposition of a nominally 91 Å thick film. Under the present experimental conditions (kinetic energy of 1000 eV) the inelastic mean free path ( $\lambda$ ) of Ti 2p electrons is about 23 Å.<sup>21</sup> Although the information depth ( $3\lambda = 69$  Å) is lower than the film thickness (91 Å) the XPS substrate signal is still clearly visible. This means that, while we can exclude the occurrence of a perfect layer-by-layer growth, we expect a growth mode characterized by the presence of islands, *i.e.* Stranski–Krastanov growth mode (layers plus islands), or Volmer–Weber growth mode (island formation).

By NEXAFS it is possible to gain information about the unoccupied states, the environment of specific chemical elements, bonding properties, and local charge distributions. NEXAFS can be described by transition matrix elements containing the dipole selection rules, thus the intensity of the NEXAFS resonances will depend on the mutual orientation of the molecular orbital involved on the given transition and the incident radiation. This aspect of the NEXAFS spectroscopy can be used to calculate the molecular orientation (angle between the molecular axis and the substrate) directly from the spectra.<sup>22</sup> Fig. 1c–e show C 1s NEXAFS spectra for different film thicknesses as indicated. The spectra were taken in p-polarization (black curves) and s-polarization (red curves) (see the experimental geometry in Fig. 1). Two main groups of resonances dominate the spectra. We can identify the  $\pi^*$ -region up to about 290 eV (dominant features 1 and 2), and the  $\sigma^*$ -region above 290 eV. Let us focus on feature 2, which is particularly sharp, in order to discuss the obtained spectra. In Fig. 1c, where the NEXAFS spectra of a 3 Å thick film are shown, we observe that the intensity of feature 2 is rather insensitive to the change of polarization of the incident radiation. This is also true for the NEXAFS spectra of a 7 Å thick film (Fig. 1d). On the contrary, a strong dichroism is clearly observable for a 24 Å thick film (Fig. 1e). This is also confirmed when calculating the molecular orientation:<sup>23</sup> we find a tilt angle of 74° for the latter film, while it is around 50° for the former. In other words, we observe an increase of the molecular orientation with the tendency toward upright standing molecules in thicker films. The structure in the monolayer regime is more complicated. The calculated molecular orientation suggests three possible textures (note that standard NEXAFS is averaged on the area seen by the beam, in our experiment around  $50 \times 100 \mu\text{m}^2$ ): (i) 50° is the real molecular arrangement. (ii) The first layer is a disordered

film. (iii) The film is characterized by small domains with differently distributed orientation. The XPS results have already shown that the first layers on top of the substrate have a poorer degree of order than the following layers. Matching XPS and NEXAFS results, we can therefore exclude that the molecules really accommodate themselves with their axis having a 50° angle with respect to the substrate. Furthermore, the comparison of the NEXAFS spectra of the first layer and the thicker films excludes the occurrence of a chemical bond. As a matter of fact, in that case, the monolayer spectra would exhibit a change in the intensity of the feature in the  $\pi^*$  region. Such a decrease in intensity of the  $\pi^*$ -resonances is not observed for a pure van-der-Waals bond between substrate and adsorbate, because this does not involve  $\pi^*$  orbitals like, for example, the LUMO or the LUMO + 1, thus there is no effect on the transitions from C 1s levels to those same orbitals. In our case, there is neither an indication of such a broadening nor an intensity reduction for resonance 2 when comparing monolayer and multilayer spectra. Consequently, we may exclude a chemical bond as a cause for the difference in structure of the first layer. This result also implies that the coupling between the  $\pi$  system of the DIP molecules and the TiO<sub>2</sub>(110) substrate is weak. This observation is in good agreement with the passivated nature of the substrate (the preparation was performed to minimize the presence of oxygen vacancies), and the fact that the rutile TiO<sub>2</sub>(110) surface is less reactive in comparison with the other TiO<sub>2</sub> crystallographic faces.

To further characterise the structure, X-ray reflectivity measurements of the DIP thin films were performed (Fig. 2). Similarly to DIP growth on other rough substrates<sup>9</sup> two Bragg reflections at  $q_z = 0.37 \text{ \AA}^{-1}$  and  $q_z = 1.47 \text{ \AA}^{-1}$  indicate the polycrystalline structure of the thin films. The Bragg reflections can be assigned to the  $\sigma$ -phase at  $q_z = 0.37 \text{ \AA}^{-1}$  (standing molecules) and to the  $\lambda$ -phase at  $q_z = 1.47 \text{ \AA}^{-1}$  (lying molecules), respectively.<sup>4</sup> Rocking scans on both Bragg reflections were measured to probe the thin films for the orientation distribution of the crystallites of each phase. The rocking curve belonging to the  $\lambda$ -phase exhibits a large mosaicity with an angular distribution width of 6.2° (FWHM). In comparison, the angular distribution width of the  $\sigma$ -phase

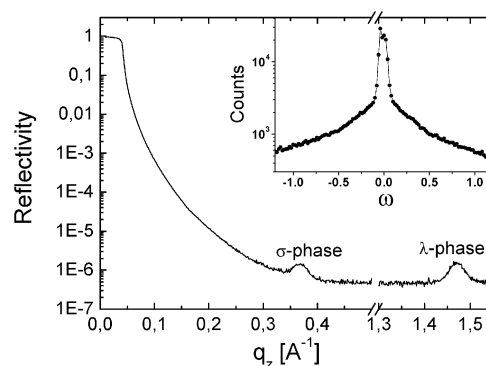


**Fig. 2** X-Ray reflectivity data from a nominally 56 Å thick DIP film showing two Bragg reflections, which can be assigned to the  $\sigma$ -phase (standing molecules) and  $\lambda$ -phase (lying molecules) of DIP. The inset shows the narrow rocking width of the  $\sigma$ -phase Bragg reflection, indicating the low mosaicity of this phase.

is very small:  $0.08^\circ$  (inset of Fig. 2), which indicates low mosaicity. These observations are consistent with the NEXAFS measurements, where a molecular tilt angle of  $\sim 50^\circ$  is found for thin films measured and highly oriented DIP molecules are found in higher thicknesses.

The  $\text{TiO}_2(110)-(1 \times 1)$  surface is characterized by parallel rows of Ti atoms running along the [001] direction, alternated with rows of bridging oxygen atoms.<sup>14</sup> The oxygen atoms protrude above the surface plane and they dominate the surface topography. Density functional theory calculations performed on benzene, pyridine and derivatives have shown that there is the possibility for those molecules to adsorb both in upright standing and in flat lying configuration on rutile  $\text{TiO}_2(110)$ .<sup>14,23</sup> The two configurations may occur simultaneously. In particular, the most stable configuration for pyridine is the upright standing one with the carbon atoms interacting with the bridging oxygen atoms *via* a hydrogen bond, while flat lying molecules are found in the [001] direction. Also in this case, there is not a chemical bond; the major role in the adsorption is played by van-der-Waals interactions, and the molecules are rather mobile. We may reckon that an analogous situation occurs when depositing DIP on  $\text{TiO}_2(110)$ : the bridging oxygen atoms force a part of the molecules impinging the surface into the upright standing position, while a part stays flat on the substrate and it is free to move probably along the [001] direction, as discussed for pyridine and acenes.<sup>14,24</sup> Also for DIP, the upright

arrangement of the molecular axis is expected to be the most energetically favourable, since the molecules in the single crystal are known to assume this configuration with respect to the cleavage plane.<sup>25</sup> This also explains the reason why the degree of order is higher in the thicker films: the influence of the substrate becomes weaker and the molecules minimize their energy according to the 3D fashion. Atomic force microscopy (AFM) images of DIP deposited on  $\text{TiO}_2(110)$  clearly reveal the island formation we expected from the XPS results (Fig. 3a). We observe that the islands are separated by regions where DIP forms layers suggesting Stranski–Krastanov growth mode (see, as an example, the profile analysis in Fig. 3b). In addition, we observe that the molecules assemble themselves in parallel crystallites, with lateral dimensions up to  $400 \text{ nm} \times 200 \text{ nm}$  that adopt the  $[1\bar{1}0]$  crystallographic axis as a preferential orientation. This effect has been also found for *para*-sexiphenyl deposited on this same substrate.<sup>26</sup> However, the reason of the crystallite orientation remained unresolved. Thus, in order to find a possible explanation, we have also investigated the bare substrate morphology after preparation by AFM. We observe in the AFM micrographs the presence of steps along the  $[1\bar{1}0]$  direction (Fig. 3c). As a consequence, the molecules are forced to nucleate islands along that direction, which also determines the elongation of the crystallite and their preferential orientation.

We have investigated DIP molecules deposited on rutile  $\text{TiO}_2(110)$  single crystals. We have found that the films, under

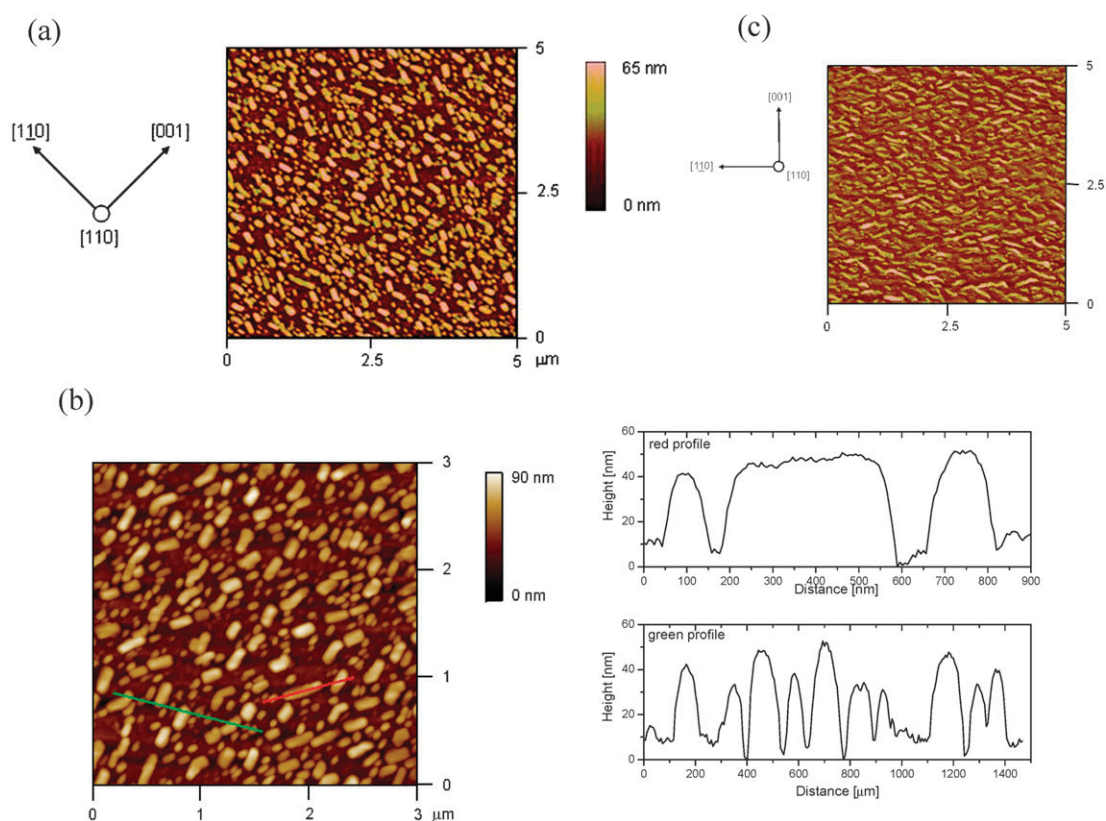


**Fig. 3** (a)  $5 \mu\text{m} \times 5 \mu\text{m}$  AFM images of nominally  $56 \text{ \AA}$  thick DIP film deposited on  $\text{TiO}_2(110)$ . The corresponding substrate azimuthal directions are also given. (b)  $3 \mu\text{m} \times 3 \mu\text{m}$  AFM images of nominally  $56 \text{ \AA}$  thick DIP film: profile analysis of the same sample. The profiles were extracted as indicated by the lines. (c)  $5 \mu\text{m} \times 5 \mu\text{m}$  AFM images of  $\text{TiO}_2(110)$  after preparation. The corresponding substrate azimuthal directions are also given.

these preparation conditions, follow a Stranski–Krastanov or Volmer–Weber growth mode. The molecules are physisorbed on the substrate. The bridging oxygen atoms influence the degree of order, presumably *via* a hydrogen bond, in the first layer on top of the substrate, and various arrangements of the molecular axes are found also in the few successive layers. The thicker films are characterized by a high orientational order with upright standing molecules. In addition, due to the substrate morphology after preparation, DIP forms crystallites preferentially oriented along the  $[1\bar{1}0]$  crystallographic axis of the substrate. Our results show the important role played by the substrate in electronic structure, molecular orientation, and morphology in the system DIP/TiO<sub>2</sub>(110) and they confirm it represents an interesting candidate for use in organic electronics. Comparing these results with previous works,<sup>14,15,24,26</sup> we conclude that the structural and morphological properties of the interface of organic thin films deposited on rutile TiO<sub>2</sub>(110) are driven by the substrate surface topography, with its rows of bridging oxygen atoms, while the molecular properties are less relevant.

The authors thank BESSY for providing beamtime, BESSY staff, in particular the Users support, and Matthias Mast. We also thank David Batchelor, and Stefan Pohl, for support at the beamline. Francesco Allegretti, University of Graz, is gratefully acknowledged for helpful discussions on rutile TiO<sub>2</sub>(110) surface preparation. We are grateful to Wolfgang Neu for his kind technical support. Financial support by BMBF under contract 05 ES3XBA/5 and by Ministerium für Wissenschaft, Forschung und Kunst Baden-Württemberg, under contract AZ 24-7532.23-21-18/2 is gratefully acknowledged.

## References

- 1 D. Braga and G. Horowitz, *Adv. Mater.*, 2009, **21**, 1473.
- 2 S. R. Forrest, *Org. Electron.*, 2003, **4**, 45.
- 3 M. B. Casu, X. Yu, S. Schmitt, C. Heske and E. Umbach, *J. Chem. Phys.*, 2008, **129**, 244708.
- 4 S. Kowarik, A. Gerlach, S. Sellner, F. Schreiber, L. Cavalcanti and O. Konovalov, *Phys. Rev. Lett.*, 2006, **96**, 125504.
- 5 S. Kera, M. B. Casu, K. R. Bauchspieß, D. Batchelor, Th. Schmidt and E. Umbach, *Surf. Sci.*, 2006, **600**, 1077.
- 6 S. Kowarik, A. Gerlach and F. Schreiber, *J. Phys.: Condens. Matter*, 2008, **20**, 184005 and references therein.
- 7 G. Witte and C. Woll, *J. Mater. Res.*, 2004, **19**, 1889 and references therein.
- 8 N. Karl, *Synth. Met.*, 2003, **133–134**, 649.
- 9 A. C. Dürr, N. Koch, M. Kelsch, A. Rühm, J. Ghijsen, R. L. Johnson, J.-J. Pireaux, J. Schwartz, F. Schreiber, H. Dosch and A. Kahn, *Phys. Rev. B*, 2003, **68**, 115428.
- 10 S. Sellner, A. Gerlach, F. Schreiber, M. Kelsch, N. Kasper, H. Dosch, S. Meyer, J. Pflaum, M. Fischer and B. Gompf, *Adv. Mater.*, 2004, **16**, 1750.
- 11 M. B. Casu, I. Biswas, M. Nagel, P. Nagel, S. Schuppler and T. Chassé, *Phys. Rev. B: Condens. Matter Mater. Phys.*, 2008, **78**, 075310.
- 12 M. B. Casu, I. Biswas, B.-E. Schuster, M. Nagel, P. Nagel, S. Schuppler and T. Chassé, *Appl. Phys. Lett.*, 2008, **93**, 24103.
- 13 A. C. Dürr, N. Koch, M. Kelsch, A. Rühm, J. Ghijsen, R. L. Johnson, J.-J. Pireaux, J. Schwartz, F. Schreiber, H. Dosch and A. Kahn, *Phys. Rev. B: Condens. Matter Mater. Phys.*, 2003, **68**, 115428.
- 14 U. Diebold, *Surf. Sci. Rep.*, 2003, **48**, 53 and references therein.
- 15 F. H. Jones, *Surf. Sci. Rep.*, 2001, **42**, 75 and references therein.
- 16 F. Allegretti, S. O'Brien, M. Polcik, D. I. Sayago and D. P. Woodruff, *Phys. Rev. Lett.*, 2005, **95**, 226104.
- 17 A. Schöll, Y. Zou, Th. Schmidt, R. Fink and E. Umbach, *J. Phys. Chem. B*, 2004, **108**, 14741.
- 18 M. L. Rocco, M. Haeming, D. R. Batchelor, R. Fink and E. Umbach, *J. Chem. Phys.*, 2008, **129**, 074702.
- 19 A. Schöll, Y. Zou, M. Jung, Th. Schmidt, R. Fink and E. Umbach, *J. Chem. Phys.*, 2004, **121**, 10260.
- 20 J. A. Venables and J. Liu, *J. Electron Spectrosc. Relat. Phenom.*, 2005, **143**, 205.
- 21 S. Tanuma, C. J. Powell and D. R. Penn, *Surf. Interface Anal.*, 1988, **11**, 577.
- 22 J. Stöhr and D. Outka, *Phys. Rev. B: Condens. Matter Mater. Phys.*, 1987, **36**, 7891.
- 23 M. B. Casu, P. Cosseddu, D. Batchelor, A. Bonfiglio and E. Umbach, *J. Chem. Phys.*, 2008, **128**, 14705.
- 24 S. Reiß, H. Krumm, A. Niklewski, V. Staemmler and Ch. Wöll, *J. Chem. Phys.*, 2002, **116**, 7704.
- 25 M. A. Heinrich, J. Pflaum, A. K. Tripathi, W. Frey, M. L. Steigerwald and T. Siegrist, *J. Phys. Chem. C*, 2007, **111**, 18878.
- 26 G. Koller, S. Berkebile, J. R. Krenn, G. Tzvetkov, G. Hlawacek, O. Lengyel, F. P. Netzer, C. Teichert, R. Resel and M. G. Ramsey, *Adv. Mater.*, 2004, **16**, 2159.